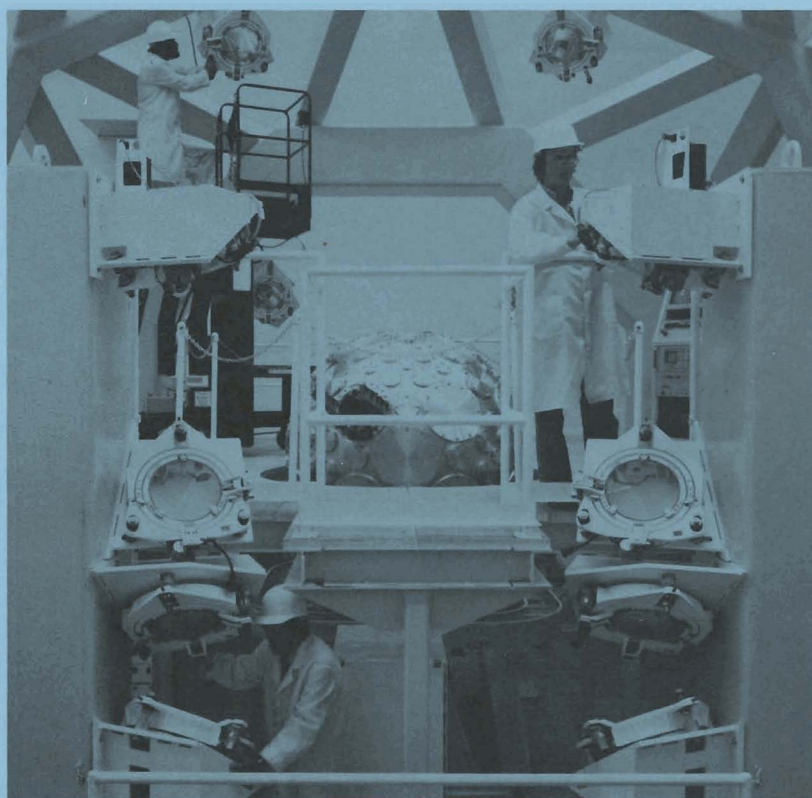


# LLE Review

## Quarterly Report



March, 1980 – May, 1980

Laboratory for Laser Energetics  
College of Engineering and Applied Science  
University of Rochester  
250 East River Road  
Rochester, New York 14623



# LLE Review

## Quarterly Report

*Editor:* **L. M. Goldman**  
**(716-275-5285)**

March, 1980 – May, 1980

---

Laboratory for Laser Energetics  
College of Engineering and Applied Science  
University of Rochester  
250 East River Road  
Rochester, New York 14623





## IN BRIEF

The period from March through May of 1980 has produced several significant advances at LLE. Probably the most important was the clear demonstration of high efficiency conversion of 1.054  $\mu\text{m}$  laser radiation to its third harmonic at .35  $\mu\text{m}$ .

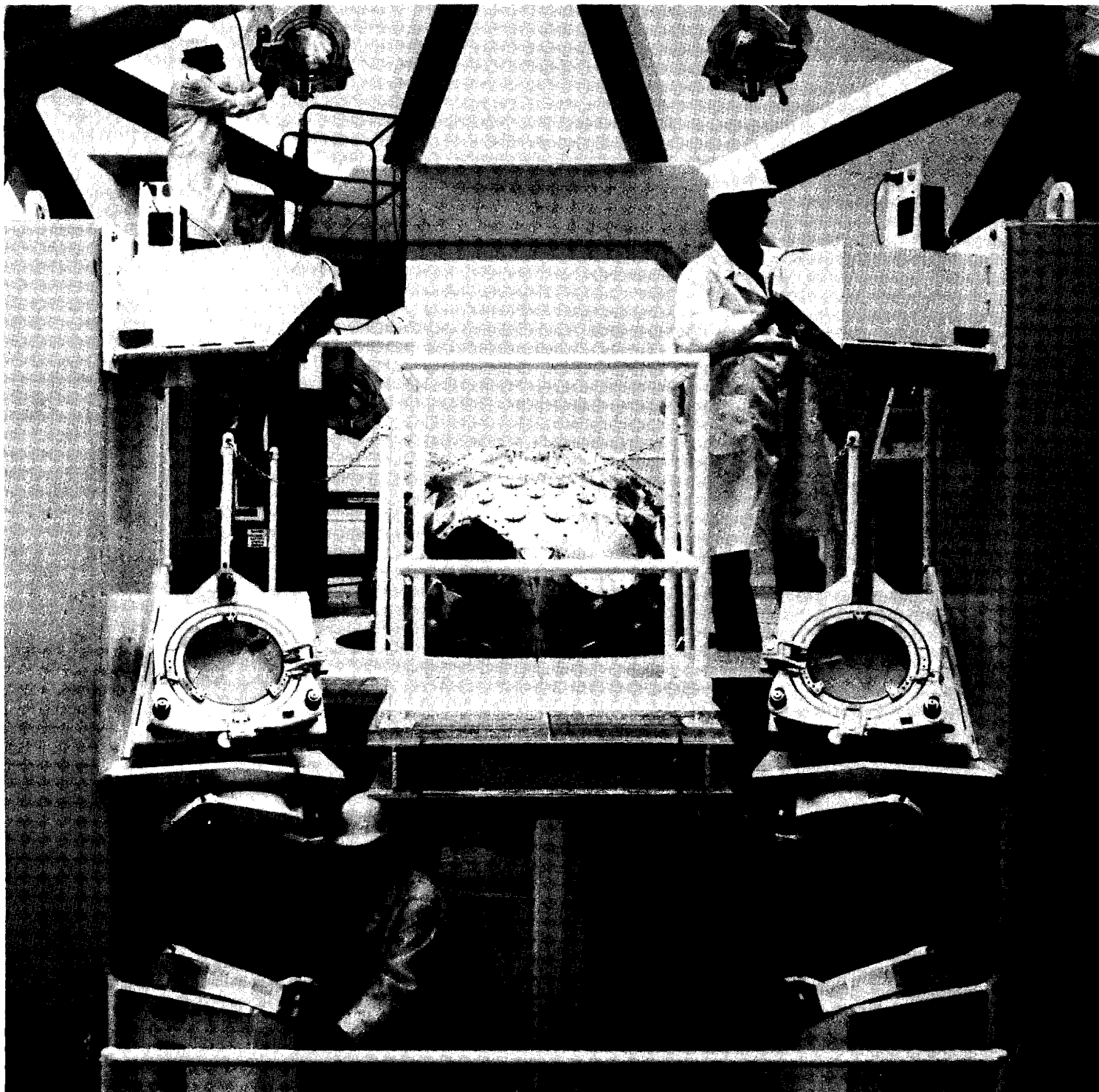
Active mirror amplifiers have been tested in both single and multiple pass configurations and have performed up to our most optimistic expectations.

Using a boosted GDL laser output of 230 J, we have demonstrated the ability to make good quality x-ray diffraction images from several biological samples with less than nanosecond exposure.



# CONTENTS

|   | <i>Page</i> |
|---|-------------|
| IN BRIEF .....  | iii         |
| CONTENTS .....  | v           |
| Section 1 LASER SYSTEMS REPORT.....   | 1           |
| 1. A Laser Wavelength Conversion<br>Program at LLE .....  | 1           |
| 1. B Tests of Double Pass Geometry<br>Using Active Mirrors .....  | 5           |
| Section 2 PROGRESS IN LASER FUSION.....   | 8           |
| 2. A A Direct Measurement of Fuel $\rho R$ .....  | 8           |
| 2. B Advances in Target Characterization<br>Computerized Methods for<br>Laser Fusion Target Analysis..... | 12          |
| Section 3 PROGRESS IN BIOPHYSICAL RESEARCH...   | 15          |
| 3. A Application of Nanosecond X-Ray<br>Diffraction Techniques to<br>Bacteriorhodopsin .....              | 15          |
| PUBLICATIONS AND CONFERENCE PRESENTATIONS ...   | 20          |
| REFERENCES .....  | 22          |



*The cover photograph shows engineers at the Laboratory for Laser Energetics aligning the mirrors on the OMEGA target chamber support structure. The mirrors direct each of OMEGA's twenty-four beams to an input port on the target chamber so that the beam can be focused on the target. The target chamber can be seen in the center of the photograph. OMEGA target shots are scheduled for September.*

## Section 1 LASER SYSTEMS REPORT

### 1.A Laser Wavelength Conversion Program at LLE

Volume 2 of the LLE Review discussed the desirability of using shorter wavelength lasers for laser fusion. In that report it was shown that it was possible to convert  $1.054\ \mu\text{m}$  radiation to its second harmonic at  $.527\ \mu\text{m}$  with high efficiency and, even more important, it was shown that it is possible to predict with great accuracy the performance of such a doubling system. We may now report that we have successfully extended this program to the third harmonic at  $.35\ \mu\text{m}$  with experimental observation of greater than 60% overall conversion efficiency from  $1.054\ \mu\text{m}$  to  $.35\ \mu\text{m}$ . This implies that an optimized system with no reflection losses would have an overall efficiency of up to 80 percent.

It is important to note that for lossless non-linear crystals the theory of non-linear conversion predicts that it is possible to convert  $1.054\ \mu\text{m}$  laser radiation at constant power to its third harmonic at  $.35\ \mu\text{m}$  with almost 100% efficiency. The most important parameter in the third harmonic generation is the mixing ratio of  $2\omega$  (green) to  $1\omega$  (red) intensity. From a quantum mechanical point of view, photons must interact one for one; therefore, an ideal tripling system will mix one photon of green light with one of

red to produce one photon in the "blue" at 3500 Å. This implies that the intensity of the green should be twice that of the red upon entering the second (mixing) crystal. Figure 1 illustrates the sensitivity of the overall tripling efficiency as a function of the mixing ratio for a particular choice of a KDP Type II crystal. These and the other theoretical predictions were calculated using the LLE code MIXER. A successful tripling program, therefore, requires that one find a doubling arrangement which converts red to green with 67% efficiency over a wide intensity range.

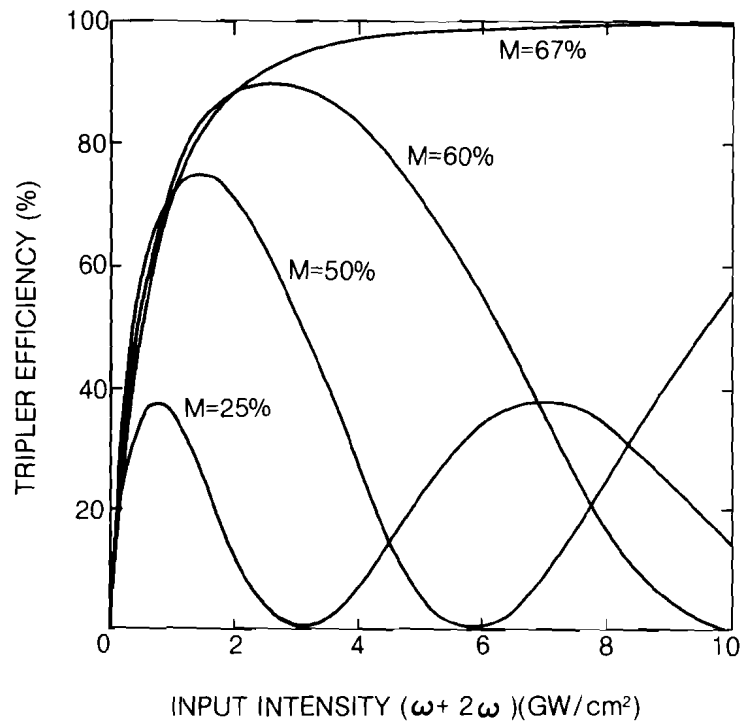


Figure 1 *Tripling efficiency of a 9 mm thick phase-matched KDP Type II crystal as a function of total input intensity, for various percentages ("mixes")  $M$  of second harmonic in the input. A small absorption of  $0.04 \text{ cm}^{-1}$  is included for the fundamental.*

TC682

Three different methods of accomplishing this result are illustrated in Figure 2. The C scheme, labeled Polarization-Bypass Scheme for Type I crystals, is the simplest to understand. Type I crystals only double the ordinary wave; therefore, if the doubling crystal is oriented for best phase matching but the polarization is adjusted so only 67% of the red light is in the ordinary beam, the conversion efficiency can be at most 67%. The doubling crystal is chosen to be sufficiently thick that most of the ordinary red light is converted to green. The other 33% of the red light, polarized in the extraordinary direction, passes through the crystal undisturbed and the desired 2:1 ratio of green energy to red is achieved at the tripler input.

The B scheme, labeled the Polarization-Mismatch Scheme, uses two Type II crystals. Again the input extraordinary beam contains 33% of the red energy. A Type II doubling crystal combines photons in the ordinary and extraordinary beams one for one; if the doubler thickness is chosen appropriately, all the energy in the extraordinary wave will combine with half of the energy in the ordinary wave to give green light, with a conversion efficiency of 67%. The other 33% of the initial red energy emerges from the doubler as unconverted ordinary light. Again the desired tripler input mix is obtained.

The A scheme, labeled Angle Detuning, requires a doubler which would normally achieve an excessive efficiency (i.e. more than 67%). This is detuned (typically by a few hundred microradians) to provide a doubling efficiency close to 67% over a broad intensity range. Either a Type I or a Type II crystal may be used as the doubler. Unfortunately this

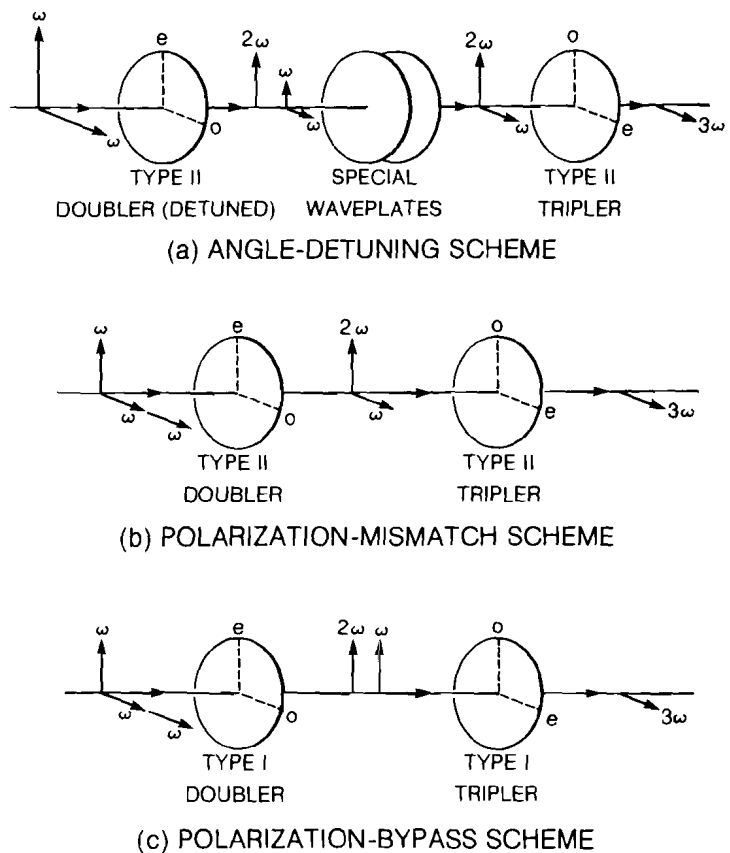
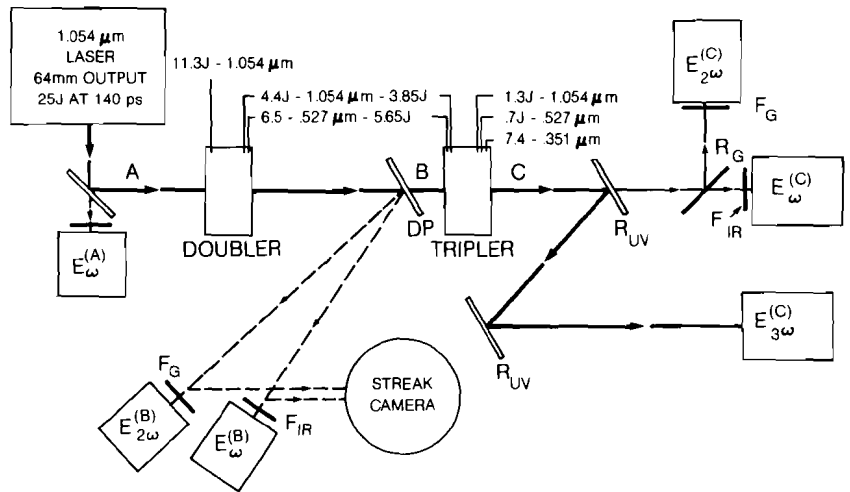


Figure 2 Idealized doubler performance for three tripling schemes. In each case two out of three ordinary photons at  $\omega$  are converted in the doubler to one extraordinary photon at  $2\omega$ . The unconverted photons at  $\omega$  emerge, respectively, (a) elliptically polarized at  $45^\circ$  to the o- and e-axes, (b) plane polarized parallel to the o-axis, and (c) plane polarized parallel to the e-axis.

TC685

Figure 3 Schematic layout of tripling experiments. Energies measured by calorimeters refer to locations A, B, and C. Quoted energies are energies just inside crystal surfaces and reflect  $\pm 2\%$  measurement accuracy. UV output is filtered by high reflectance, dielectric mirrors ( $R_{UV}$ ) only;  $R_G$  is a high-reflectance green mirror;  $F_{IR}$  and  $F_G$  are IR and green-pass filters; DP is a diagnostic (wedged) glass plate.



E920

scheme is very sensitive to errors in alignment, particularly for Type I doublers, since it does not operate on the phase-matching peak. For Type II doublers two extra waveplates are required between the crystals.

The C scheme is also sensitive to angular mismatch because it uses Type I crystals. We have therefore concentrated our experimental program on the second, Polarization Mismatch, scheme which is insensitive to angular mismatch as it operates on the phase-matching peaks of two Type II crystals. We have also tried the angle-detuning scheme and proved that it works. The measurements were made with a portion of the GDL laser system terminated at the 64 mm amplifiers. Both conversion crystals were 60 mm in diameter. The experimental arrangement is shown in Figure 3. Each of the measurements was confirmed by a redundant measurement of both the converted and unconverted light. On every shot time dependent streak measurements were taken of the red and green beams, and on some shots simultaneous streaks were obtained of all three wavelengths.

The experimental results for harmonic conversion over a wide range of intensities are shown in Figure 4. This data has been corrected for Fresnel reflection losses from the uncoated surfaces. The excellent correlation between the observations and the calculations is clear evidence for the applicability of the theory. The calculations represent an integration over both the spatial and temporal intensity profiles of the laser beams as determined from near field and streak camera measurements.

Close agreement between theory and experiment has also been obtained using crystals of different thicknesses, confirming the theoretical scaling law that the intensity at which peak tripling efficiency is attained is inversely proportional to the square root of the crystal thickness. It is therefore possible to design tripling systems to work in different regions from that shown in Figure 4.

These experiments clearly demonstrate that it is possible to convert  $1.054 \mu\text{m}$  radiation to  $.35 \mu\text{m}$  with the high efficiencies predicted by the theory.

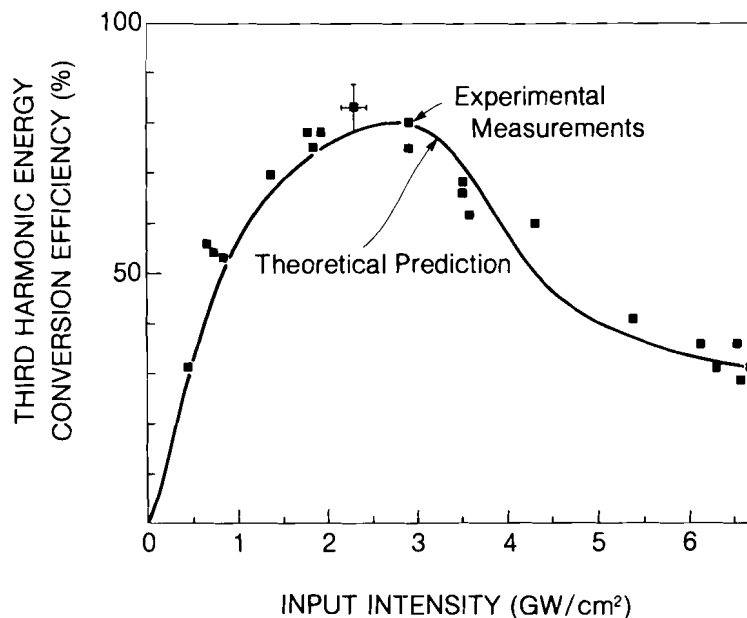
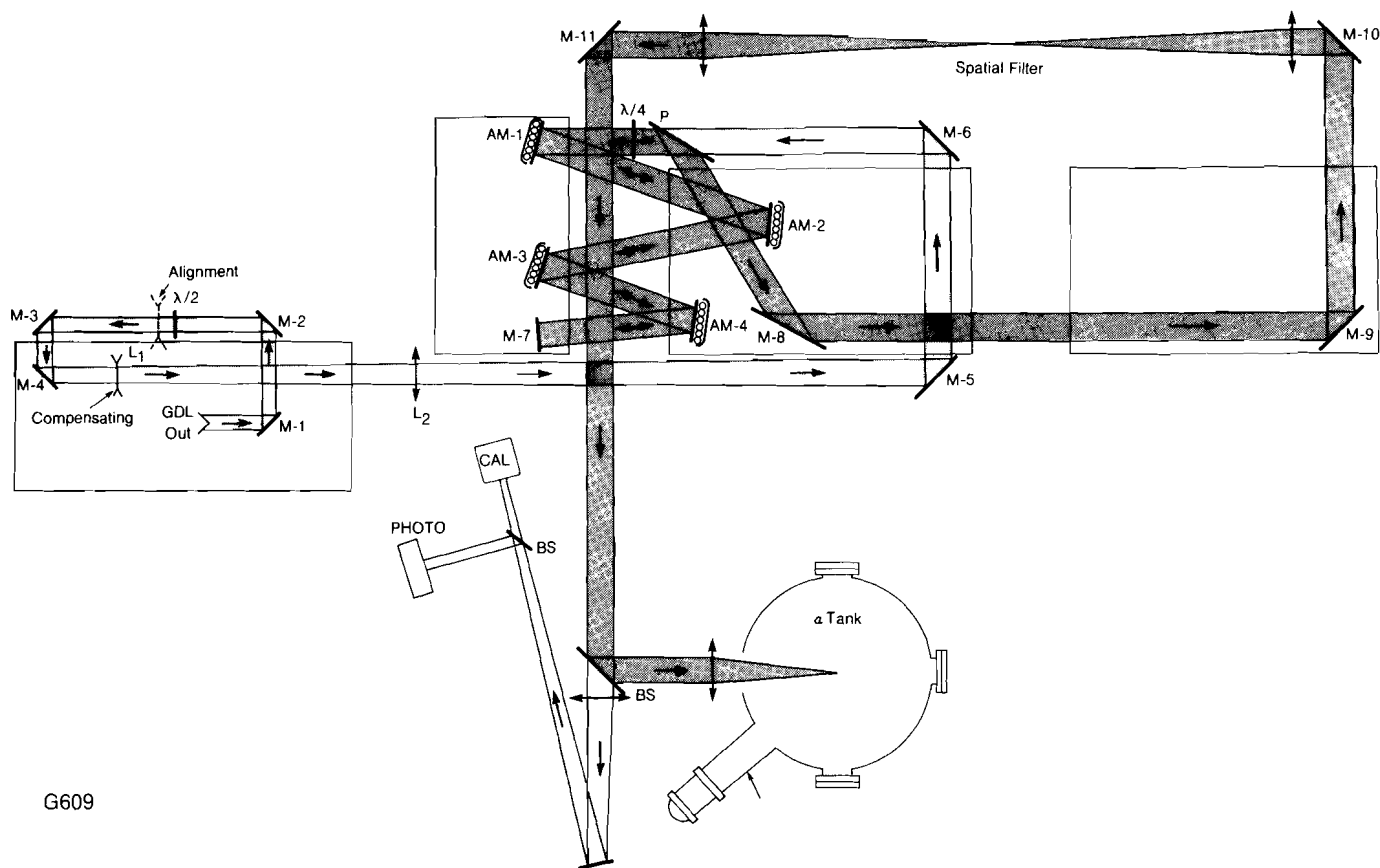


Figure 4 *Third harmonic generation efficiency for 12 mm, Type II KDP. Theoretical prediction used experimental temporal and spatial pulse shapes.*

E924

## 1.B Tests of Double Pass Geometry Using Active Mirrors

The use of multiple optical passes through the same active laser medium has been demonstrated in a number of different laser systems.<sup>1</sup> Calculations using the LLE RAINBOW propagation code suggested that multi-passing might be advantageous for a system employing "active mirror"<sup>2</sup> laser amplifiers.



G609

Figure 5 Optical configuration for long pulses (700 psec) of double pass active mirror tests.

Tests have been carried out on the GDL laser system to investigate the performance of a multipass active mirror system. The optical arrangement for the test is shown in Figure 5. The linearly "P" polarized beam coming from the 90 mm amplifiers of the one beam GDL laser is expanded from 90 mm to 150 mm in diameter and transmitted through the dielectric polarizer P. The beam is then converted to circular polarization in the  $\lambda/4$  quartz waveplate. It is then amplified in passing through active mirror elements AM-1 through AM-4, reflected at mirror M-7, and then amplified a second time in the active mirror elements. Since there are an odd number of reflections, the handedness of the circular polarization is reversed, thus providing an "S" polarized beam after passing through the quarter waveplate. This allows the polarizer P to reflect the beam into the output path containing M-8 through M-11. The output of the laser beam was used in the biophysics x-ray diffraction studies described in Section 3 of this publication.

The primary advantage of the double pass method is in improving the extraction efficiency of each amplifier disc.

Extraction efficiency is important for longer pulses so these tests were carried out with 700 picosecond pulses. At long pulse widths the energy limitation of the system was determined by material damage to the dielectric coatings on the active mirror units and on the 1/4 wave plate. For these tests the front face of AM-1 was uncoated while the other units used standard LLE anti-reflection coatings.

The system was fired for a total of 111 high power laser shots over a period of four weeks. The performance of the system is shown in Figure 6. The observed output energy versus input energy for the double pass system is shown in the upper curve. The continuous line is the prediction of the propagation code RAINBOW. The lower curve shows the performance of the same four 15 cm active mirror units operating in a single pass configuration. The excellent correlation between the measured and calculated values indicates that the system performs in a predictable fashion. The maximum output energy is the same for the single and double pass arrangement since it is determined by energy loading on the output amplifier surfaces. The obvious advantage of the double pass configuration is demonstrated by the reduced driver energy needed for a given output.

It was not possible to determine detailed beam quality in this series of measurements due to surface damage initially present in some of the optics used in these experiments. The output data, however, were all measured beyond a 5 meter spatial filter with a 2 mm pinhole.

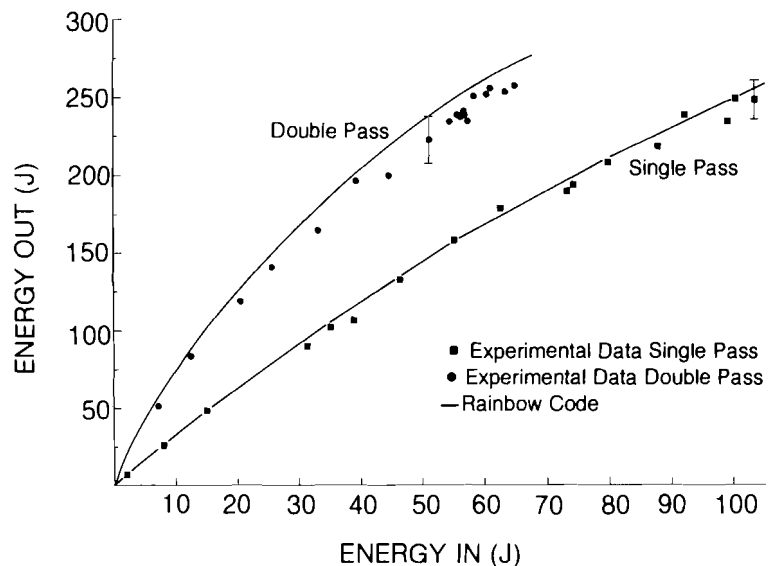


Figure 6 Comparison of experimental observations with RAINBOW code predictions for single and double pass operation of four 15 cm active mirror units.

G615

## Section 2 PROGRESS IN LASER FUSION

### 2.A A Direct Measurement of Fuel $\rho R$

We are examining a new diagnostic that provides a direct measurement for  $\rho R$  in the DT fuel<sup>3,4,5</sup>. The method uses the fact that 14 MeV neutrons, produced in DT fusion reactions, can elastically scatter from one of the deuterium or tritium ions before leaving the fuel region. The number of such knock-on reactions is directly proportional to the  $\rho R$  of the fuel, and thus, a measurement of their number represents a direct determination of the fuel  $\rho R$ .

The relation between the number of knock-ons and fuel  $\rho R$  is determined in the following way: the number of elastic collisions  $Q$  produced by  $Y$  14 MeV neutrons is:

$$Q = (N_d \sigma_d + N_t \sigma_t) \langle R \rangle Y$$

Here,  $N_d$  and  $N_t$  are the number densities for deuterium and tritium;  $\sigma_d$  and  $\sigma_t$  are the respective cross sections for elastic scattering with a 14 MeV neutron (.92 and .62 barns); and  $\langle R \rangle$  is the average distance for a neutron to traverse the fuel. For equimolar DT this expression yields:

$$\rho \langle R \rangle = 5.4 Q/Y \text{ g/cm}^2$$

Thus, the ratio of the number of knock-ons to the number of 14 MeV neutrons determines  $\rho R$  of the fuel.

Knock-on deuterons and tritons can be detected with the solid-state track-detector, CR-39.<sup>6</sup> One possible experimental configuration is shown in Figure 7. The first tantalum filter is used to block ions from the blow-off plasma and 3 MeV protons from the DD reaction. About 20% of the knock-on particles will penetrate the filter. Of these, about 1/2 will be in the energy window of the track detector. Determining the fraction of detected knock-ons is an essential part of the diagnostic and will be discussed below. There is no need to separate the deuteron and triton signals.

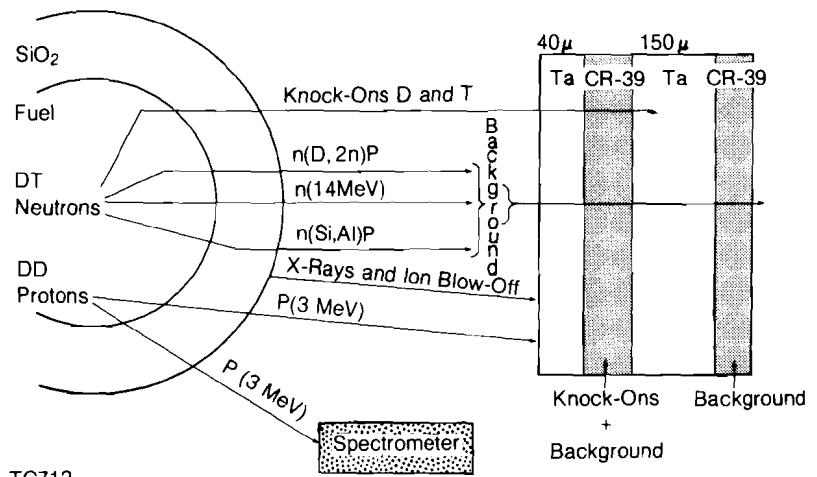


Figure 7 Schematic of the knock-on  $\rho R$  measurement experiment.

Some sources of background are also shown in Figure 7. These include the production of protons from (n,p) reactions by neutrons in the fuel, tamper, filter, and track detector. The tracks produced by all these reactions are estimated to be considerably less than the knock-on signal. Further, some of the background tracks can be separated out easily according to their diameter or trajectory. The amount of other background tracks can be estimated by using a filter thick enough to stop the knock-on signal but not the background from high-energy protons. This background can then be measured with an additional track detector.

A possible source of background not shown in Figure 7 is MeV protons that can be produced from the laser-target interaction. These can be produced even from nominally

hydrogen-free targets—presumably from contamination on the surface. Energies greater than 3 MeV are necessary to produce a background signal. Such energetic protons have been observed at Livermore<sup>4</sup>, but not from the ZETA laser system. If they should occur on the higher power Omega system, it will be necessary to employ target cleaning techniques within the target chamber before each shot.

An essential part of the diagnostic is determining what fraction of the knock-ons have been detected by the track detector. A difficulty arises because the knock-ons are produced with a continuum of energies (0 - 10.6 MeV for tritons), resulting from different neutron impact parameters. Further, the energy spectrum has peaks and valleys due to an anisotropic differential cross section for elastic scattering. There is no a priori way to know which part of the spectrum will be in the energy window of the track detector, as the spectrum can be shifted and distorted due to energy loss in the target (mainly the tamper). An example of how the fraction of detected knock-ons varies with tamper density and temperature is shown in Figure 8. The results were obtained from computer simulations which calculated the distortion and shift of the knock-on spectrum as it moved through the fuel, tamper and tantalum filter. Windows for

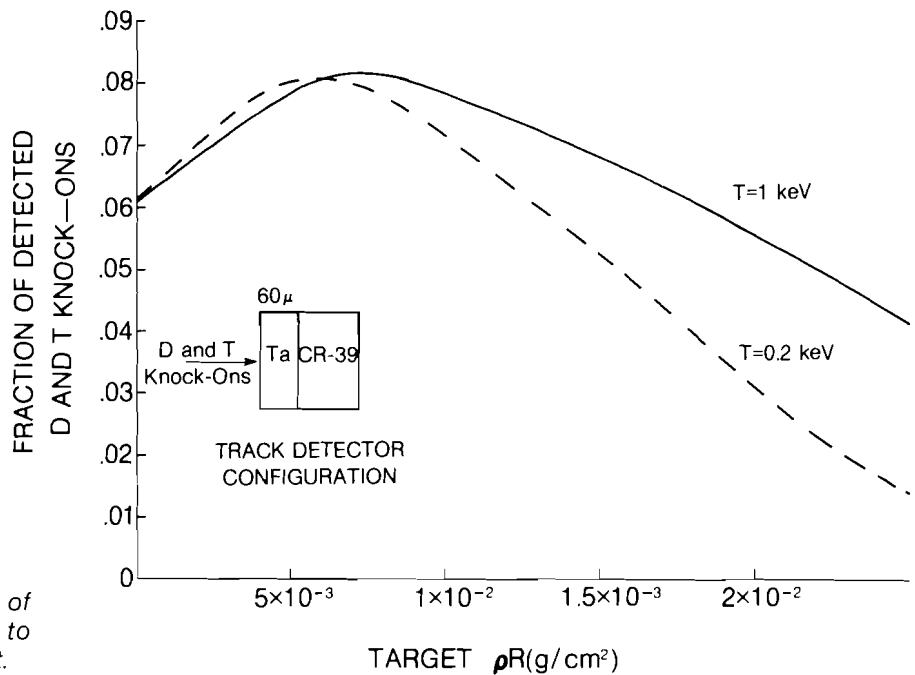


Figure 8 Variation in the fraction of detected knock-ons due to energy loss in the target.

TC721

the track detectors have been determined to be 2-4 MeV for deuterons and 3-6 MeV for tritons. Different windows will change the results quantitatively, but the qualitative features will remain the same.

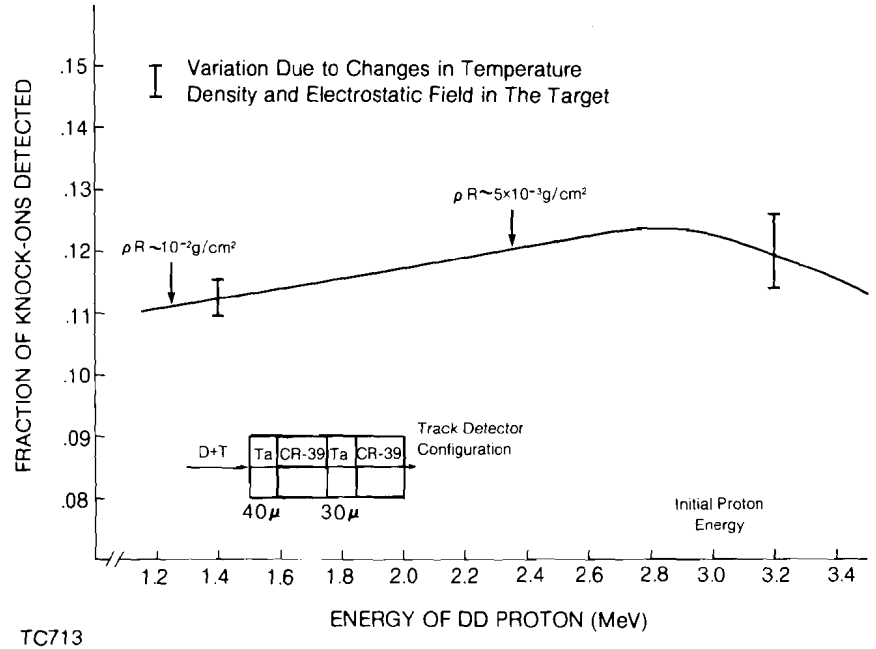
A 60  $\mu\text{m}$  Ta filter was found to be optimum for the low to medium  $\rho R$  cases,  $0 < \rho R \lesssim 10^{-2} \text{ g/cm}^2$ . In this range the fraction of detected knock-ons was found to vary by about  $\pm 15\%$ , which will introduce the same percentage error in the inferred value for fuel  $\rho R$ . The reason for variation is that the part of the spectrum in the track-detector window changes from a valley to a peak and back to a valley as  $\rho R$  increases. The tantalum thickness chosen shows the minimum variation.

The uncertainty in this  $\rho R$  range can be reduced in two ways: 1) by correlating the fraction of knock-ons with the energy loss of protons produced in the DD fusion reaction (3.02 MeV), and 2) by using a double track-detector configuration. DD protons are useful because their velocity is very close to the velocity of the knock-on particles detected in Figure 8. Hence, their energy loss is very similar to the energy loss of the knock-ons and determines fairly well which part of the spectrum is in the track detector window. The variation with  $\rho R$  can be smoothed with a double track-detector configuration. It can be adjusted so that when the knock-on peak moves out of one detector, it enters the other.

Results for a double track-detector configuration are shown in Figure 9. As seen, the variation is now so smooth that correlation with the DD proton is not even necessary. However, it is necessary to at least see the proton because the curve drops off sharply for target conditions that stop the proton, i.e.  $\rho R \gtrsim 0.02 \text{ g/cm}^2$ . The error bars show the variation that can result from different temperatures in the tamper and from electrostatic fields that can be produced by the laser-target interaction<sup>7</sup>. Over the range,  $\rho R \lesssim 0.01 \text{ g/cm}^2$ , the uncertainty is only about 5% which makes this diagnostic look very attractive for near term experiments.

For higher  $\rho R$ , we can no longer use the DD protons to correlate distortion of the knock-on spectrum, as they will be absorbed in the target. Instead, we can use protons from secondary  $\text{He}^3$  - D reactions, which should be sufficiently

Figure 9 Correlation between the fraction of D and T knock-ons detected and the energy of DD protons. To first order the DD proton is proportional to the  $\rho R$  of the fuel plus tamper. Note the fraction varies less than ten percent from  $\rho R$  of 0.02 down to  $\rho R$  of  $10^{-4}$ .



numerous for detection. With these, the diagnostic can be extended to the threshold of thermonuclear ignition,  $\rho R \sim .2 \text{ g/cm}^2$ . Above this value knock-on particles will generally not escape the target.

## 2.B Advances in Target Characterization Computerized Methods for Laser Fusion Target Analysis

A new technique has been developed for characterization of transparent laser fusion targets. Target microballoons are placed in one arm of a modified Mach-Zehnder interferometer as shown in Figure 10. The interferometer is different from conventional interferometers in the manner with which the wave front is measured. Conventional interferometers use photographs of the fringe pattern which are interrogated with a microdensitometer and a computer to reconstruct the wave front. The disadvantage of this is the long time ( $\sim$  hours) required for measurement. The modified interferometer<sup>8</sup> uses a modulated mirror to vary temporally the phase of the wave front. The mirror is

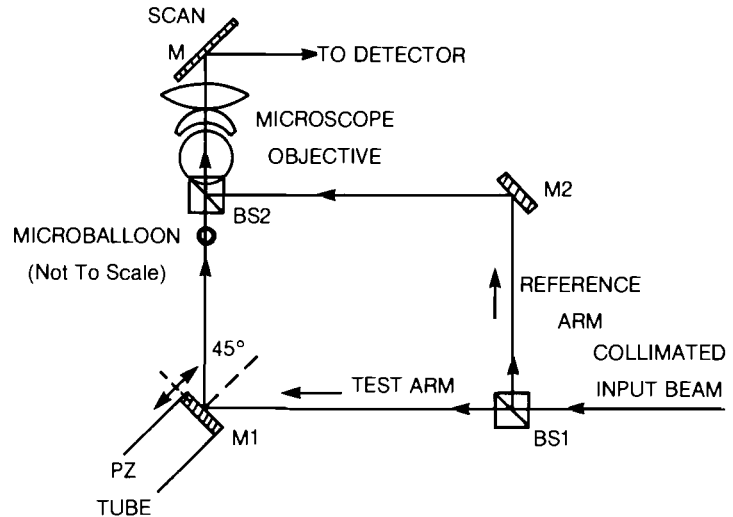


Figure 10 Optical arrangement for AC interferometry of microballoons.

T198

driven at 20kHz over a fraction of a wavelength by a piezoelectric crystal. A photodiode detecting the modulated wave front is used to determine the phase at a point in the wave front. The image of the wave front is scanned across the detector creating a map of the wave front in real time.

The use of this type of interferometer makes possible the measurement of the wave front in a few seconds. Figure 11 illustrates a typical wave front measured in this manner.

The wave front data is processed by a mini-computer which makes use of the large number of data points to determine the average target diameter to  $\pm 4\%$  and average wall thickness to  $\pm .03$  microns. These tolerances are based experimentally on the use of 1000 data points in the wave front. They could be improved with more data points. The advantages this method offers over manual measurements are: a shorter measurement time, more objectivity in the measurement, automatic storage of the wave front for later study, and the potential for complete automation.

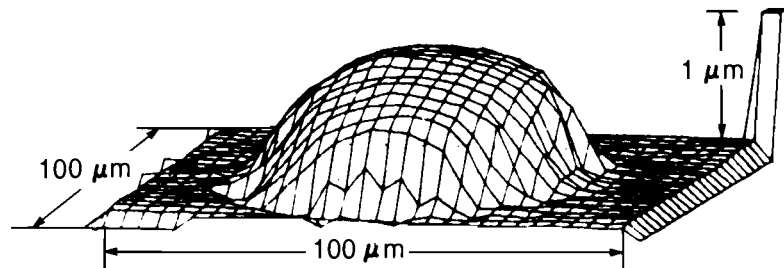


Figure 11 Perspective representation of a microballoon wavefront.

T141

In the above method no new information is obtained over that obtained with conventional<sup>9</sup> manual methods. Use of a microballoon manipulator<sup>10</sup> as shown in Figure 12 will allow characterization of the change in wall thickness over the microballoon. A manipulator of this type has been fabricated and run under computer control. The microballoon is rotated by synchronously moving the pads in opposite directions. Because there is no differential motion, the center of the microballoon remains fixed in space. The pads are made of a soft material which allows pressure to be placed on the microballoon without damaging it. With the microballoon held in the interferometer a map of wall thickness versus polar position may be generated. This technique has already been used for visual inspection of the whole surface of microballoons.

An additional use of the modified Mach-Zehnder interferometer is for measuring the pressure retention of microballoons. In a 100 micron microballoon a change of 2 atmospheres of Argon gas can be measured. This is twice the resolution of conventional interference microscopes. Three independent measurements allow an iterative solution of the fill pressure and the pressure half life. This technique is very useful in testing the effectiveness of new gas sealing methods.

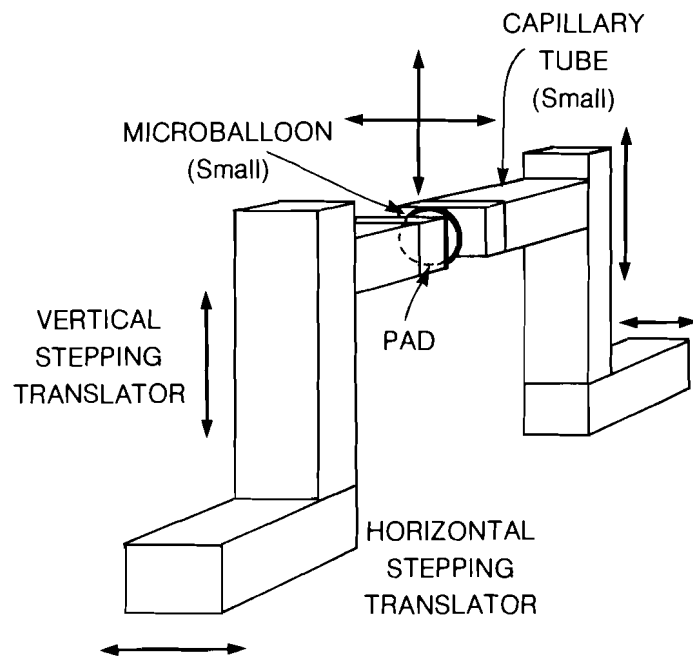


Figure 12 Schematic arrangement of microballoon manipulator.

T199

## Section 3

# PROGRESS IN BIOPHYSICAL RESEARCH

### 3.A Application of Nanosecond X-Ray Diffraction Techniques to Bacteriorhodopsin

The use of x-ray diffraction methods to investigate atomic structures in biological macro molecules has been common for many years<sup>11</sup>. In the past, because of the long exposure times needed for good quality records, the measurements have almost all been of static subjects. With the advent of intense x-ray sources from laser produced plasmas, it becomes possible to make x-ray diffraction measurements with sub nanosecond exposures. As an illustration, we are preparing to adopt x-ray diffraction techniques to study the photo response of bacteriorhodopsin in purple membrane.

The bacteriorhodopsin (BR) in the purple membrane (PM) of the halobacterium halobium has been clearly demonstrated to be a light activated photon pump<sup>12</sup>. One particular issue under debate involves the magnitude of any conformational change that may take place during the BR photocycle. We hope to contribute to the resolution of this question by using the newly developed laser plasma x-ray source<sup>13</sup> to obtain subnanosecond x-ray diffraction patterns throughout the course of the 20 millisecond photocycle.

The x-ray diffraction patterns discussed above require approximately  $10^{10}$  photons of nearly monochromatic light. It has been demonstrated in many laboratories that laser produced plasmas are reasonably efficient producers of soft x-ray radiation. With the proper choice of target materials and laser intensity, a large part of the x-ray radiation may be channelled into a few narrow emission lines<sup>14</sup>. For x-ray diffraction studies, x-ray sources in the 4.5 Å - 1.5 Å region of the spectrum with a spectral spread of less than 1% are appropriate.

To generate the purple membrane diffraction pattern discussed below, the single beam Nd<sup>+3</sup> Glass Development Laser at the University of Rochester's Laboratory for Laser Energetics (LLE)<sup>15</sup> was used. This laser delivers single pulses of 1.054 μm light with full width at half maximum that can be varied from 50 - 700 psec. With newly added active mirror booster amplifiers<sup>16</sup> peak pulse powers of greater than 1 TW have been obtained with short pulses and a maximum energy of 250 joule with long pulses. The laser output aperture was 15 cm. Our system repetition rate was 2 pulses/hour.

Laser pulses were brought to a focus of 100 μm in a 24 inch diameter vessel which was evacuated to  $1 \times 10^{-5}$  Torr. Plasmas must be produced in a vacuum to prevent air breakdown before the laser light reaches the surface of the target.

Attached to the target chamber was an x-ray camera (shown in Figure 13) consisting of a nickel coated grazing reflection toroidal mirror<sup>17</sup> with a focal length of 62.5 cm and a mean angle of incidence of 0.91 degrees. The collection solid angle of the collector was  $2.4 \times 10^{-4}$  steradians. The system also included an annular aperture in the reflected x-ray beam, a controlled environment sample chamber, a controlled environment sample chamber, an annular aperture in the reflected x-ray beam, a controlled environment sample chamber,

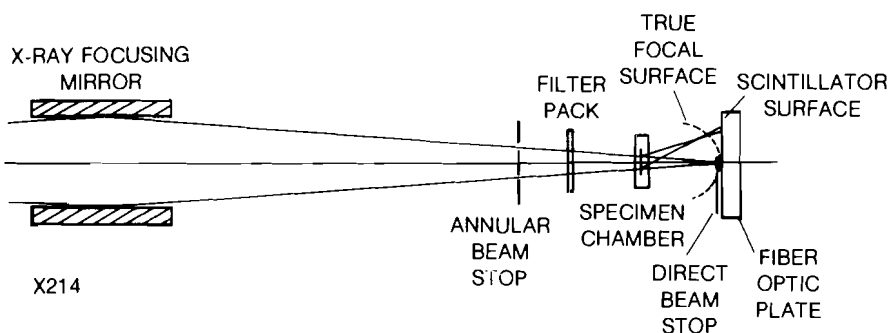


Figure 13 Schematic diagram of x-ray diffraction camera. The true focal surface of the camera is a sphere tangent to the sample and also tangent to the flat phosphor plane.

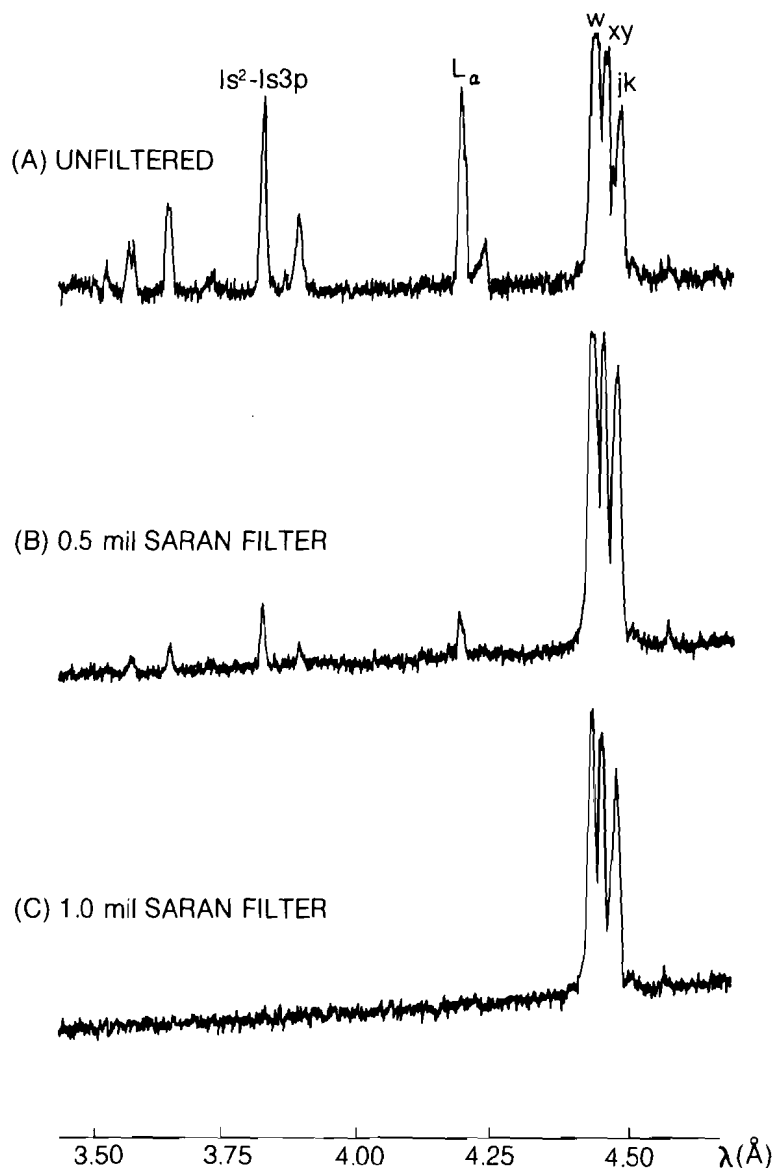
and a scintillator-image intensifier recording system. The 40 mm ZnS (Ag) scintillator was located 125 cm from the laser plasma source and was coupled to an Amperex model XX1360 25 mm channel plate intensifier through a fiberoptic faceplate. The intensifier had an adjustable luminosity gain of up to  $7 \times 10^4$  and was housed in a mount permitting direct attachment of various 35 mm and Polaroid camera backs. A lead disc 2.5 mm in diameter was mounted just in front of the scintillator plane to block the direct beam from the x-ray mirror.

Our experiments so far have been performed with highly chlorinated targets; room temperature saran ( $C_2H_2Cl_2$ ) and pressed polycrystals of hexachloroethane ( $C_2Cl_6$ ) held at 77°K (low temperature inhibits hexachloroethane sublimation in the vacuum chamber) have been used. In a saran plasma produced by irradiation with an incident 175J, 700 psec laser pulse focussed to  $\sim 10^{15}$  watts/cm<sup>2</sup>, about  $5 \times 10^{-4}$  of the incident laser energy (or  $\sim 3 \times 10^{14}$  photons) is radiated by  $Cl^{+15}$  at 4.45 Å in a wavelength interval of  $\Delta\lambda/\lambda$  of  $8 \times 10^{-3}$ . Since x-ray production by plasma ions is proportional to the ion density, the hexachloroethane produces about twice the x-ray flux of saran. For simplicity, however, saran was the target used in most test shots.

A typical emission spectrum from a saran plasma is shown in Figure 14a. In addition to the intense line radiation at 4.45 Å we have x-ray lines at shorter wavelengths and a much weaker background continuum. Effective monochromatization of this emission is possible by means of thin saran foils. Such filtered spectra are shown in Figures 14b and 14c corresponding to 12.5 μm and 25 μm foil thicknesses, respectively. The 25 μm foil transmits 57% of the desired line radiation. Outside the spectral range shown in Figure 14 we filter the long wavelength components with a 25 μm beryllium foil while the short wavelength radiation is not reflected by the toroidal mirror.

Figure 15 shows an x-ray powder diffraction pattern from a PM stack recorded on 2475 high speed recording film. It was obtained with a single 700 psec 220 joule pulse focussed on an hexachloroethane target; the camera collected  $\sim 3-4 \times 10^9$  photons for diffraction. The identifiable reflections are noted. The diffraction rings are indexed on a 2-dimensional P-3 hexagonal lattice<sup>18</sup>. Typical high quality PM powder patterns have been obtained using rotating

Figure 14 Chlorine spectra from saran targets on three different laser shots showing the effect of saran filtration. All shots were approximately 170 J in 700 psec. The  $Cl^{+15}$  resonance line (w) and its associated satellites (x, y, j, k) are the components useful for x-ray diffraction. The  $1s^2-1s3p$  is a higher energy  $Cl^{+15}$  emission line. The  $L\alpha$  is radiated from  $Cl^{+16}$  ions. Filtration for (A) was 25  $\mu m$  Be; for (b) 25  $\mu m$  + 12/5  $\mu m$  saran; for (c) 25  $\mu m$  saran. In (C) the transmission of the resonance line and its satellites was 57% while all other lines were almost completely absorbed.



X216

anode tube sources and exposure times of 20 - 50 hours<sup>19,20</sup>. In these patterns strong rings out to 7 Å resolution are observed, while weaker rings out to 3.5 Å are also seen. In our pattern the lower resolution orders are well resolved and quite intense. They extend out to a resolution of ~ 15 Å and are good enough for quantitative data reduction and structure determination. The high resolution orders, although intrinsically as bright as the lower orders are out of focus in Figure 15. This is primarily because the scintillator used in this experiment was deposited on a flat fiber optic surface. The actual focal surface of the x-ray camera is a sphere tangent to the sample and to the mirror focus<sup>17</sup> as shown in Figure 13.

In a time resolved experiment, a master timing signal will generate an electrical pulse, and initiate a green laser stimulus pulse to a hydrated purple membrane stack situated in the humid sample chamber of the x-ray camera. Then, after a delay ranging from nanoseconds to tens of milliseconds, the main laser will fire, generating plasma-produced x-rays which will yield an x-ray diffraction pattern. By varying the delay, a stroboscopic series of diffraction patterns will be obtained.

The information contained in these powder patterns can be used along with the phase information obtained from electron diffraction studies to yield a two dimensional projection of the electron density of the purple membrane perpendicular to the plane of the membrane. This view offers a great deal of information about the bacteriorhodopsin (BR) because the seven helices of the BR are arrayed roughly perpendicular to the membrane plane. That is, the projection looks down the helical chains. Hence, for example, in a dynamic experiment conformational changes involving movement of the helices may be readily apparent.

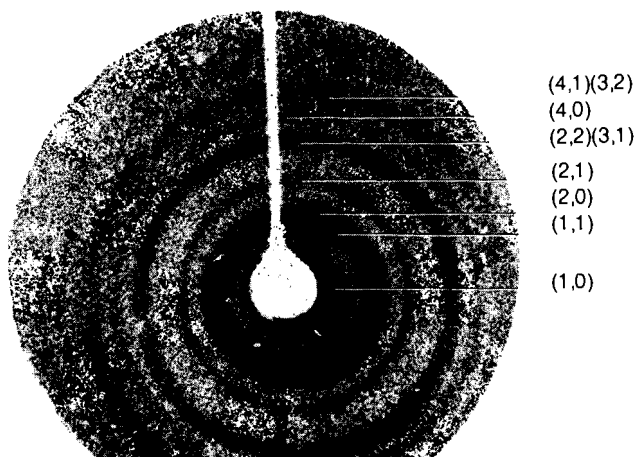


Figure 15 *Purple membrane diffraction pattern. The sample-phosphor separation was 2.7 cm. Identified are rings indexed on a hexagonal lattice. Higher resolution rings are out of focus due to spherical focal plane of the camera.*

LASER PULSE ENERGY - 213 Joules    X-RAY SOURCE -  $\text{Cl}^{+15}$  LASER HEATED PLASMA  
 LASER PULSE WIDTH - 700 psec    X-RAY WAVELENGTH - 4.45 Å

X209

## PUBLICATIONS AND CONFERENCE PRESENTATIONS March 1980 – May, 1980

### Publications

1. "Symmetric Laser Compression of Argon-Filled Glass Shells to Densities of 4-6 g/cm<sup>3</sup>," B. Yaakobi, S. Skupsky, R.L. McCrory, C.F. Hooper, H. Deckman, P. Bourke, and J.M. Soures; *Physical Review Letters* **44**, 16 (April 1980) 1072-75.
2. "X-Ray Line Shift as a High Density Diagnostic for Laser-Imploded Plasmas," S. Skupsky; *Physical Review A* **21**, (April 1980) 1316-26.

### Forthcoming Publications

1. "High Density Effects on Thermonuclear Ignition for Inertially Confined Fusion", Stanley Skupsky; submitted for publication in *Phys. Rev. Letters*.
2. "X-Ray Absorption Fine Structure Measurement Using Laser Compressed Target as a Source", B. Yaakobi, H. Deckman, P. Bourke, S. Letzring, J.M. Soures; submitted to *Applied Physics Letters*.

3. "Time Resolved Spectroscopy of Large Bore Xe Flash-lamps for Use in Large Aperture Amplifiers", John H. Kelly, David C. Brown, and Kenneth Teegarden; submitted for publication to *Applied Optics*.
4. "Theory of High Efficiency Third Harmonic Generation of High Power Nd: Glass Laser Radiation", R.S. Craxton; accepted for publication by *Optics Communications*.
5. "Demonstration of High Efficiency Third Harmonic Conversion of High Power Nd:Glass Laser Radiation", W. Seka, S.D. Jacobs, J.E. Rizzo, R. Boni, and R.S. Craxton; accepted for publication by *Optics Communications*.
6. "X-Ray Absorption Lines: Signature for Preheat Level in Non-Explosive Laser Implosions", B. Yaakobi, R.L. McCrory, S. Skupsky, P. Bourke, and J.M. Soures; accepted for publication by *Optics Communications*.
7. "Electrooptic Prepulse Suppression for Fusion Laser Systems", G. Mourou, J. Bunkenburg, W. Seka; accepted for publication by *Optics Communications*.
8. "Picosecond Time Delay Fluorimetry Using a Streak Camera", Michael Stavola, Gerard Mourou, Wayne Knox; accepted for publication by *Optics Communications*.
9. "Soft X-Ray Population Inversion in Laser-Plasmas by Resonant Photo Excitation and Photon Assisted Processes", V.A. Bhagavatula; accepted for publication by *Journal of Quantum Electronics*.

## REFERENCES

1. K. Brueckner, S. Jorna, K. Moncar, *Applied Optics* **13**, 2183 (1974).
2. J. A. Abate, L. Lund, D. Brown, S. Jacobs, S. Refermat, J. Kelly, O. Lewis, M. Gavin, S. Waldbillig, paper submitted to *Applied Optics* (1980).
3. S. Skupsky, LLE Internal Memo (May, 1978).
4. N.M. Ceglio, private communication (November, 1978); N.M. Ceglio and E.V. Benton, UCRL-82550 (January, 1980).
5. D.C. Slater, KMSF-U-914 (1980).
6. Y.V. Rao, A. Davis, R.C. Filey, P.J. McNulty, and D. Shirkey, *Bulletin of American Physical Society* **24**, 650 (1979).
7. Y. Gazit, J. Delettrez, T.C. Bristow, A. Entenberg, and J. Soures, *Physical Review Letters* **43**, 1943 (1979).

8. G.W. Johnson, D.C. Leiner, and D.T. Moore, *Optical Engineering* **18**, 46 (1979).
9. B.W. Weinstein, *Journal of Applied Physics* **46**, 5305 (1975).
10. J.A. Monjes, B.W. Weinstein, D.L. Willenborg, and A.L. Richmond, UCRL-83375.
11. R. Henderson and P.N.T. Unwin, *Nature* **257**, 28 (1975).
12. D. Oesterhelt and W. Stoeckenius, *Proceedings of the National Academy of Science* **70**, 2853 (1973).
13. R.D. Frankel and J.M. Forsyth, *Science* **204**, 622 (1979).
14. J.M. Forsyth, *Transactions of the American Crystallographic Society* **12**, 11 (1976).
15. W. Seka, J. Soures, O. Lewis, J. Bunkenburg, D. Brown, S. Jacobs, G. Mourou, and J. Zimmerman, *Applied Optics* **19**, 409 (1980).
16. J.A. Abate, L. Lund, D. Brown, S. Jacobs, S. Reformat, J. Kelly, M. Gavin, S. Waldbillig, and O. Lewis, submitted to *Applied Optics* (1980).
17. B.L. Henke and J.W.M. DuMond, *Journal of Applied Physics* **26**, 903 (1955).
18. A.E. Blaurock and W. Stoeckenius, *Nature New Biology* **233**, 152 (1971).
19. R. Henderson, *Journal of Molecular Biology* **93**, 123 (1975).
20. A.E. Blaurock, *Journal of Molecular Biology* **93**, 139 (1975).

This report was prepared as an account of work conducted by the University of Rochester ('U of R') sponsored in part by the Empire Electric Research Corporation ('ESEERCO'), the General Electric Company ('GE'), Exxon Research and Engineering Company ('Exxon'), the Standard Oil Company (Ohio) ('SOHIO'), the New York State Research and Development Authority ('NYSERDA'), Northeast Utilities ('NU'), and the Department of Energy ('DOE'). Neither ESEERCO, GE, Exxon, SOHIO, NYSERDA, NU, DOE, nor the U of R, nor their members or employees, nor any persons acting on their behalf either:

- a. Makes any warranty of representation, express or implied, with respect to the accuracy, completeness, or usefulness of the information contained in this report, or the use of any information, apparatus, method, or process disclosed in this report may not infringe privately owned rights ; or
- b. Assume any liability with respect to the use of, or for damages resulting from the use of, any information, apparatus, method or process disclosed in this report.



